Scientific Journal of Impact Factor (SJIF): 4.72

e-ISSN : 2348-4470
p-ISSN : 2348-6406

International Journal of Advance Engineering and Research Development

National Conference On Nanomaterials, (NCN-2017)

Volume 4, Special Issue 6, Dec.-2017 (UGC Approved)

Effect of pH on Thermoelectric Oxide $Ca_3Co_4O_9$

S. Berbeth Mary[1], D. Edward Christy[2] A. Panithra Amuthini[1], A. Leo Rajesh[1*]

[1]*Department of Physics, St.Joseph's College (Autonomous), Tiruchirappalli-620 002, Tamil Nadu, India.*
[2] *Research Scholar, Research and Development Cenre, Bharathiyar University, Coimbatore – 641046, Tamil Nadu, India.*

Abstract*The misfit layered cobalt oxide $Ca_3Co_4O_9$ is a promising thermoelectric material prepared through different potential of hydrogen (pH) ranging from 8 – 10 by citric acid complexing coupled with hydrothermal method by varying the pH level of the solution followed by annealing at 800°C. The effect of PH variation on the structural, morphological, compositional and optical properties of $Ca_3Co_4O_9$ nanoparticles were characterized by using X - ray diffractometer, Scanning Electron Microscopy, Fourier Transform Infrared Spectroscopy and UV-Visible Spectroscopy. Identical crystal phases were obtained from XRD analysis and the average crystallite size decreased with increasing pH level, it was found to be 78, 61, 56 nm by using Scherrer formula. Morphological studies confirmed the increment of crystallite size due to rapid nucleation of larger pH value and the porous nature of the samples also found. Strong peak identified at 564 cm^{-1} revealed the formation of metal oxides by FTIR spectroscopy. The results of the optical absorption studies showed that the indirect band gap energy values of the calcium cobaltite nanoparticles decreased from 3.22 eV to 2.41 eV with increasing pH values*

Key words: *layered cobaltite, potential of hydrogen, thermoelectric oxide, rapid nucleation*

1. Introduction

The development of environmental friendly and cost effective power sources overcomes the problems of energy crises and global warming. Thermoelectric devices can directly convert waste heat into electricity. This technology can recover natural energy such as solar and geothermal energy, but also waste heat from industries. These devices can operate for longer durations without maintenance due to its non moving parts and it is free from global warming gas emission. The efficiency of a thermoelectric material depends on the thermoelectric figure of merit ZT [1-2]. Efficient thermoelectric materials must show high thermo power (S) to obtain a high voltage and electrical conductivity (σ)to reduce the internal resistance of the material combined with a low thermal conductivity (κ) to introduce the large temperature difference between both ends of the material. These three parameters S, σ, κ depends on each other since they are closely related to the scattering of charge carriers and lattice vibrations. The electronic, magnetic and electromagnetic properties of these oxides depend strongly on crystallite size and the oxidation state of the metal centers. Modified band structure can enhance the electrical conductivity (σ) and Seebeck coefficient (S) at the same time nanostructure reduces the thermal conductivity by increasing the phonon scattering consequently ZT gets improved. So the addition of dopants and substitutions can increase ZT values [3-8]. Intermetallics, Skutterudites, half-Heusler and chalcogenide compounds are some of the promising thermoelectric materials. However, these materials are not attractive when operating at higher temperatures due to decomposing, vaporizing and melting nature at higher temperatures. But metal oxides have attracted much attention at higher temperature on the basis of their potential advantages over heavy metallic alloys. Due to high thermal and chemical stability in air, the metal oxides are widely used as thermoelectric materials at higher temperatures [9-11]. The structure of $Ca_3Co_4O_9$ is similar to $NaCo_2O_4$, with the misfit structure of CdI_2- type CoO_2 layers stacked up with triple rock salt - type layers alternately along the c-axis. These two kinds of layers have similar a, c and β lattice parameters but different b parameter. To accentuate the inadequate nature of the structure, $Ca_3Co_4O_9$ has two monoclinic subsystems, $[Ca_2CoO_3]_{(b2/b1)}[CoO_2]$, where b_1 and b_2 are two different lattice parameters of the rock salt system and the CoO_2 subsystem respectively. The edge sharing CoO_2 octahedral layers are charge reservoir to supply charge carriers into the CoO_2 layers [12-14].

Citric acid complexing with hydrothermal method is very simple and easy to prepare $Ca_3Co_4O_9$ (CCO) nanoparticles. This method is prominently and most effective because of compositional modification, microstructure control using capping chelating agents, doping can be controlled. The amount of H^+ and OH^- ions decides the morphology by influencing the polymerization of the metal oxygen bonds during sol formation while the hydrolysis and condensation of the solution affected by the pH during gel formation. The phase formation, particle size and morphology of the structure during solution method are the consequences of varying pH of the solution [15]. This research article reports the influence of pH on

structural, morphological, compositional and optical properties of $Ca_3Co_4O_9$ by hydrothermal method for thermoelectric applications.

2. Materials and Methods

AR Grade Calcium nitrate tetrahydrate, cobalt nitrate hexahydrate, citric acid monohydrate and ammonia solution were used without further purification. Calcium Cobalt Oxide (CCO) nanopowders were prepared using the citric acid complexing coupled with hydrothermal method. Stoichiometric amounts of nitrates of calcium, cobalt and equal amount of citric acid were dissolved in deionized water so that the metal ions can be consistently complexed together. A certain amount of ammonia solution was added drop wise to the above mixed solution and part of ammonia added to defuse the unreacted citric acid. pH value of the solution was adjusted to 8, 9, and 10 respectively by adding ammonia solution, hence a sol was obtained and then this sol was transferred to a 150 ml autoclave and the autoclave was placed into an oven for hydrothermal treatment at 200 °C for 20h. The obtained precursors were in turn filtered, washed with deionized water and ethanol and then dried at 120 °C over night. The dried powders were calcined in air in a furnace at 800 °C for 4h [16].

Powder X-ray diffraction pattern has been recorded in order to identify the Phase and the crystal structure, using a XRD diffractometer (D8 Advanced) with Cu Kα radiation. Microstructural observations were performed on powder samples, using scanning electron microscopy (SEM, JEOL JSM-6700F) at 20 kV and images were obtained. The composition was characterized by FTIR spectrophotometer in the range of 4000-400cm^{-1}. The optical property of the CCO nanoparticles and band gap was determined by using a Lambda 35 UV-vis spectrometer.

3. Results and discussion

X-ray diffraction (XRD) patterns of the CCO samples at selected pH values 8, 9 and 10 are shown in Fig. 1. Amorphous nature was perceived for the sample prepared at pH 8and the pattern synthesized at pH 9 agreed well with that of the $Ca_3Co_4O_9$ (JCPDS card no 23-0110) while the sample synthesized at pH 10 concurred with $Ca_9Co_{12}O_{28}$ (JCPDS card no 21-0139). These two substances were identical in crystal phases, whereas oxygen content is differs to some extent. The composition $Ca_9Co_{12}O_{28}$ varied by one oxygen atom, results higher oxidation state for Co [17]. This may be attributable to the reduction of more Co cations from higher to lower valances accompanied by increased ionic radius and the formation of more oxygen vacancies since the average oxidation state for Co ions in $Ca_9Co_{12}O_{28}$ is higher than that of $Ca_3Co_4O_9$ [18]. The average crystallite size of the synthesized samples was calculated from the major diffraction peaks using the Scherrer formula $D = K\lambda / \beta\cos\theta$, Where K is a constant (K = 0.94), λ is the wavelength (1.5418 Å), θ is the Bragg angle and β is full width half maximum that is, broadening due to the crystalline dimensions [19]. The average particle size of the prepared samples at pH 8, pH 9 and pH 10 were calculated as 78, 61 and 56 nm respectively. The presence of the $Ca_3Co_4O_9$ phase prepared at pH 9 had a strong influence on the electrical and thermoelectric properties of CCO nanoparticles [20]. The surface to volume ratio of nanoparticles gradually increased with decreasing particle size has been observed in metal oxides with perovskite structure as of $Ca_3Co_4O_9$.

Fig. 2 signifies the surface morphology of $Ca_3Co_4O_9$ nanoparticles revealed by SEM analysis. It can be seen that the samples were composed of rod-like grains with different sizes. The grains demonstrated randomly oriented structure as expected for the typical structure of $Ca_3Co_4O_9$ ceramic materials. The relatively high degree of porosity nature was observed for the sample prepared at pH 9 due to the solid state synthetic methods. It can be seen from 3(c) that the plate like grains were more pronounced for the sample prepared at pH 10 because of rapid nucleation. Enhanced Seebeck effect and low thermal conductivity observed for the porous nanograined materials henceforth the sample prepared at pH 9 will be optimized for thermoelectric application due to its $Ca_3Co_4O_9$ phase purity and poros nature of the sample [21].

The formation of $Ca_3Co_4O_9$ phase from the precursor was further ascertained by FTIR spectroscopy as shown in fig 3. The band around 3400 cm^{-1}represnted the O-H mode of vibration and the peak broadened when there was an increment in the pH level of the solution and its movement played an important role in the structure formation where the phase changes from $Ca_3Co_4O_9$ to $Ca_9Co_{12}O_{28}$. The strong asymmetric stretching mode of vibration of C=O was observed at around 1500 cm^{-1}. As the pH value increased by the addition of alkali ammonia solution, the vibration peak of C=O shifted from up and down which implied the phase change. The symmetric stretching occurred at 850 cm^{-1} confirmed the vibration of NO_3^{-1} ions. The standard peak of CCO nanoparticles was observed at 564 cm^{-1} [22-24].

The optical properties of $Ca_3Co_4O_9$ nanoparticles were characterized by UV-vis spectroscopy. Fig.4 (a) shows the UV-visible spectrum of $Ca_3Co_4O_9$ nanoparticles. The optical band gap of $Ca_3Co_4O_9$ was strongly influenced by the size, shape, and dimension of materials. There absorption peaks in the spectrum at 208, 247 and 277 nm confirmed the formation of CCO nanoparticles at different pH values. The band gap E_g can be calculated from the equation $(\alpha h\nu)^n = B(h\nu - E_g)$, Where α is the absorption coefficient, $h\nu$ is the photon energy, B is constant, and n can be either 1/2 or 2 for indirect and direct transition respectively [25]. From the $(\alpha h\nu)^{1/2}$ versus hν curve, the band gap was found to be 3.22, 2.86, 2.41 eV respectively. The determined band gap value showed that larger band gap for the lower pH value [26].

4. Conclusion

$Ca_3Co_4O_9$ nanoparticles have been synthesized by using citric acid complexing coupled with hydrothermal method at different pH levels. Amorphous, good and low crystalline fine powders were achieved with identical phase of $Ca_3Co_4O_9$ perovskite oxide nanoparticles and there was a slight change in composition due to the different oxidation state of Co cation. pH variation altered the crystallite size as it reduced when pH increased. SEM Micrograph showed well dispersed and porosity nature sample. The peak at 564 cm^{-1} established the formation of $Ca_3Co_4O_9$ phase. The estimated band gap reduced from 3.22 to 2.41 eV while the pH of the solution increased. The $Ca_3Co_4O_9$ nanoparticles prepared at pH 9 will be optimum for thermoelectric applications.

References

1. J. P. Heremans, V. Jovovtha, E. S. Toberer, A. Saramat, K. Kurosaki, A. Charoenphakdee, S. Yamanaka, G. Snyder, J.Sci., 321,554 (2008)
2. J. Pei, G. Chen, N. Zhou, D. Q. Lu, F. Xiao, Physica B., 406, 571 (2011)
3. S. Malkhandi, B.Yang, A. K. Manohar, A.Manivannan, G. K. Surya Prakash, S.R.Narayanan, J. Phys. Chem.Lett., 3, 967 (2012)
4. C. Gayner, K. K. Kar, Prog. Mater. Sci., 83, 330 (2016)
5. S. Walia, S. Balendran, H. Nili, S. Zhuiykov, G. Rosengarten, Q. H. Wang, M. Bhaskaran, S. Sriram, M. S. Strano, K. Kalanta/r Zadeh, Prog. Mater. Sci., 58, 1143 (2013)
6. W. Liu, Q. Jie, H. Kim, Z. Ren4, Acta Mater., 87, 357 (2015)
7. F. Delorme, C. Fernandez Martin, P. Marudhachalam, O. Ovono Ovono, G. Guzman, J.Alloys.Compd., 509, 2311 (2011)
8. M. Ohtaki, H.Koga, T.Tokunga, K. Eguchi, H. Arai, J. Solid State Chem., 120, 105 (1995)
9. G. Mahan, B. Sales, J. Phys. Today., 50, 42 (1997)
10. K. F. Hsu, S. Loo, F. Guo, W. Chen, J. S. Dyck, C. Uher, T. Hogen, E. K. Polychroniadis, M. G. Kanatzidis, Science., 303, 818 (2004)
11. B. Abeles, R. Cohen, J. Appl. Phys., 35, 247 (1964)
12. Hirmochi Ohta, Kenji Sugiura, Kunihito Koumoto, Inorg. Chem., 47, 8429 (2008)
13. Yang Wang, Yu Sui, Fang Li, Luxiang Xu, Xianjie Wang, WenhuiSu, Xiaoyang Liu, J. Nanoen., 1, 456 (2012)
14. W.Koshibae, K.Tsutsui, S. Maekawa, Phys. Rew B., 62, 6869 (2000)
15. Rizwan Wahab, Young soon Kim, Hyung Shik Shin, Mater. Trans., 50, 2092 (2009)
16. Jianrong Niu, Jiguang Deng, Wei Liu, Lei Zhang, Guozhi Wang, Hongxing Dai, Hong He, Xuehong Zi, catal.Today., 126, 420 (2007)
17. H. Tran, T. Metha, M. Zellar, R. H. Jarman, Mater. Sci. Bull., 48,2450 (2013)
18. K. T. Lee, A. Manthiram , Chem. Mat., 18, 1621 (2012)
19. S. Enzo, G. Fagherazzi, A. Benedetti, S. Polizzi, J. Appl. Cryst.,21 536 (1988)
20. Masahiro Tahashi, Kiyoshi Ogawa, Makoto Takahashi, Hideo Goto, J. Cera. Soc.Jap., 121,444 (2013)
21. Hohyun Lee, Daryoosh Vasahee, Wang DZ, Mildred S Dresselhaus, Ren ZF, Gang Chen, J.Appl. Phys., 107, 94308 (2010)
22. Rizwan Wahab, Young-Soon Kim, Hyung-Shik Shin, Mater.Trans., 50, 2092 (2009)
23. R. Wahab, S. G. Ansari, H. K. Seo, Y. S. Kim, E. K. Suh, H. S. Shin, Solid State Sci., 11, 439 (2009)
24. L. Wu, Y. Wu, L. Wei, Phys. E., 28, 76 (2005)
25. M. C. Santhiosh Kumar, B. Pradeep, Indian J. Phys.,85, 401 (2011)
26. Mohamed Hamid Elsheikh, Dhafer Abdulameer Ahnawah, Mohd Faizul Mohd Sabri, Shuhana Binti Mohd Said, Masjuki Haji Hassan, Mohammed Bashir Ali Basher, Mahazani Mohamad, Rene. Sust. Ener. Rews., 30, 337 (2014)

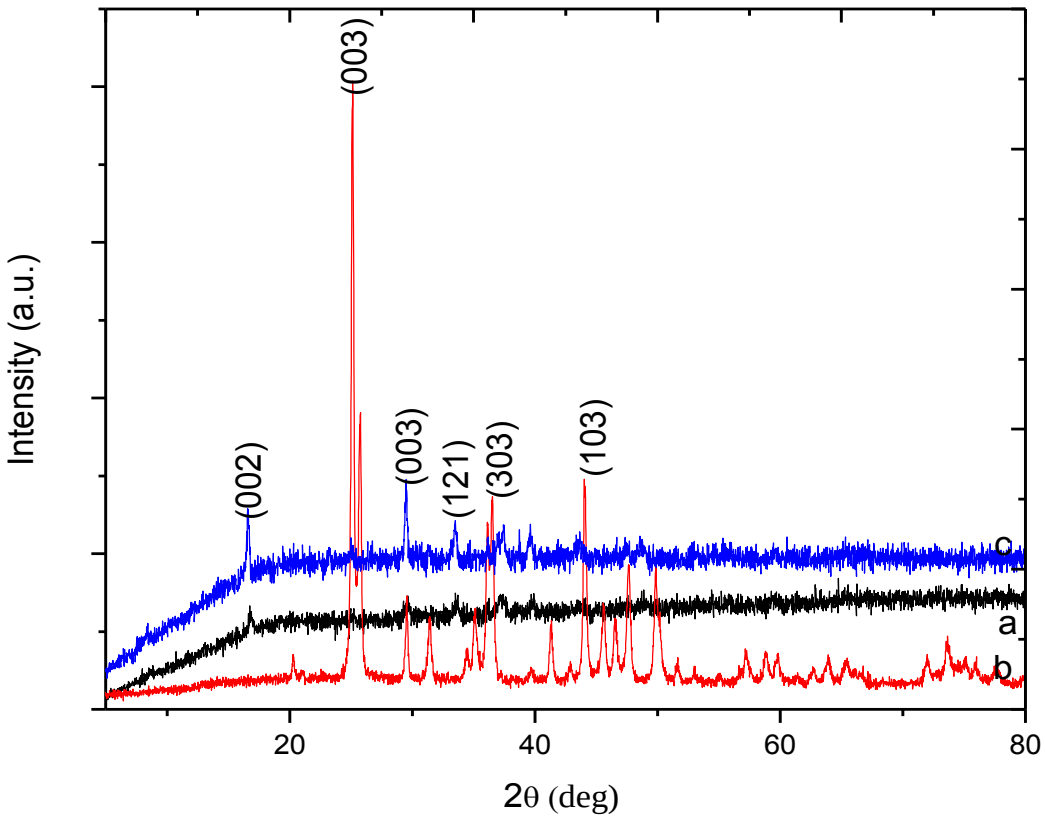

Fig.1. Powder XRD Patterns for $Ca_3Co_4O_9$ nanoparticles at (a) pH 8 (b) pH 9 (c) pH 10

Effect of pH on Thermoelectric Oxide $Ca_3Co_4O_9$
S. Berbeth Mary[1], D. Edward Christy[2] A. Panithra Amuthini[1], A. Leo Rajesh[1*]

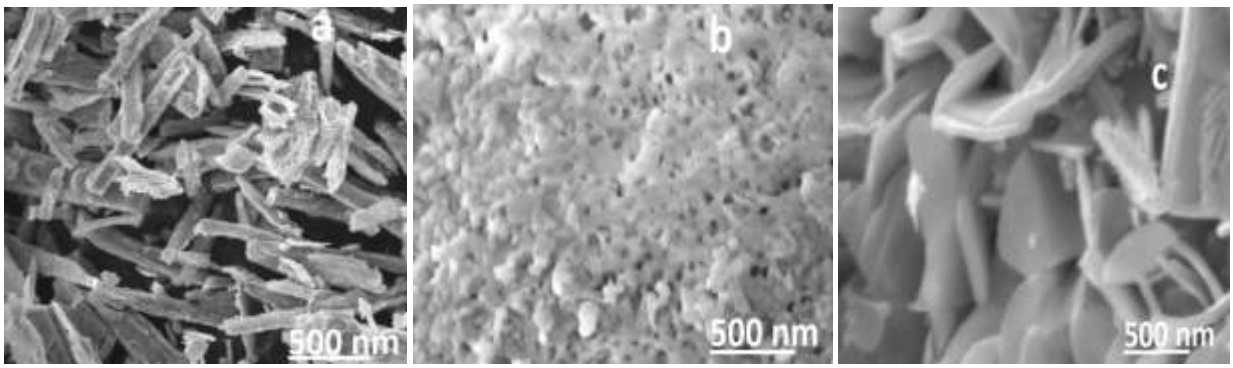

Fig.2. SEM Micrograph of $Ca_3Co_4O_9$ nanoparticles at (a) pH 8 (b) pH 9 (c) pH 10

Effect of pH on Thermoelectric Oxide $Ca_3Co_4O_9$
S. Berbeth Mary[1], D. Edward Christy[2] A. Panithra Amuthini[1], A. Leo Rajesh[1*]

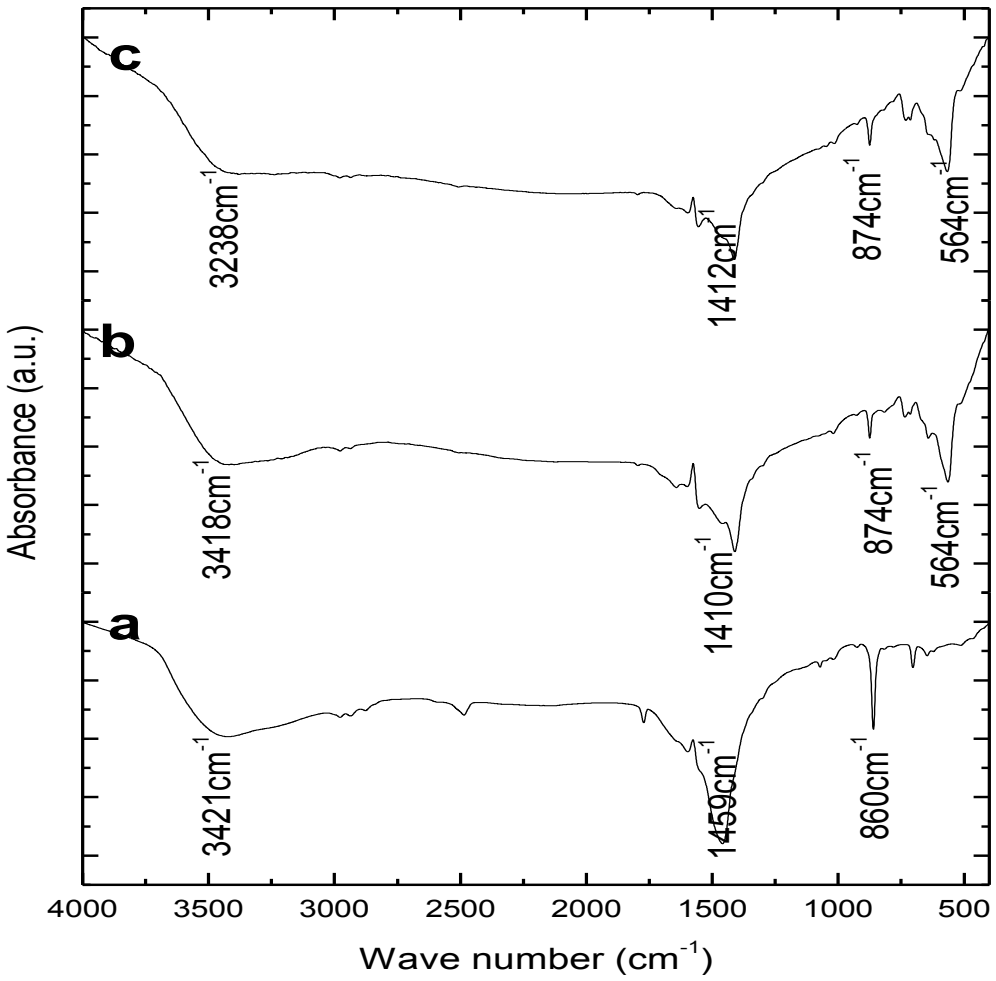

Fig.3. FTIR Spectra of $Ca_3Co_4O_9$ nanoparticles at (a) pH 8 (b) pH 9 (c) pH 10

Effect of pH on Thermoelectric Oxide $Ca_3Co_4O_9$

S. Berbeth Mary[1], D. Edward Christy[2] A. Panithra Amuthini[1], A. Leo Rajesh[1*]

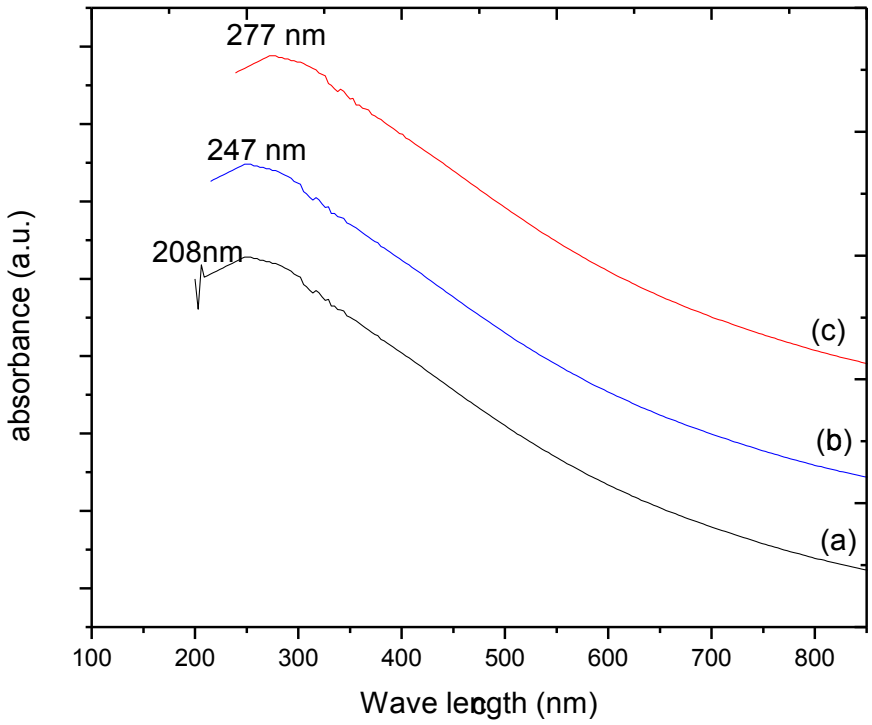

4 (a)

Effect of pH on Thermoelectric Oxide $Ca_3Co_4O_9$

S. Berbeth Mary[1], D. Edward Christy[2] A. Panithra Amuthini[1], A. Leo Rajesh[1*]

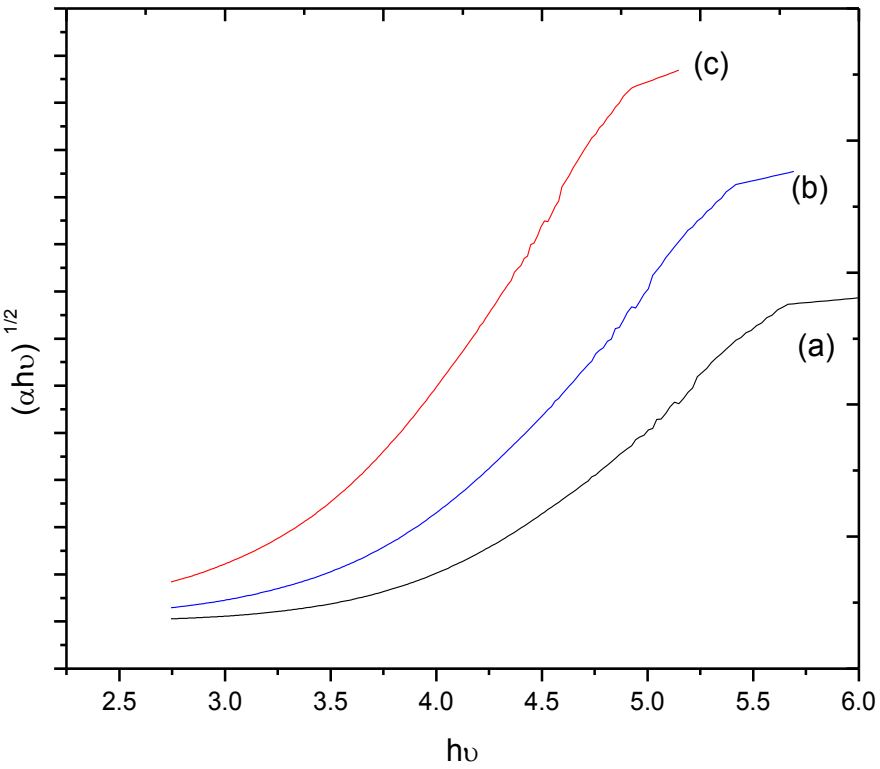

4(b)

Fig. 4(a) UV –Vis spectra of $Ca_3Co_4O_9$ Nanoparticle 4(b) Band gap determination

Effect of pH on Thermoelectric Oxide $Ca_3Co_4O_9$

S. Berbeth Mary[1], D. Edward Christy[2] A. Panithra Amuthini[1], A. Leo Rajesh[1*]

